Remote Sensing of Environment 113 (2009) 610–621

Contents lists available at ScienceDirect

Remote Sensing of Environment

journal homepage: www.elsevier.com/locate/rse

Spectral optimization for constituent retrieval in Case 2 waters II: Validation study in the Chesapeake Bay

C.P. Kuchinke [a], H.R. Gordon [a,*], L.W. Harding Jr. [b], K.J. Voss [a]

[a] Department of Physics, University of Miami, PO Box 248046, Coral Gables, Florida 33124, USA
[b] Horn Point Laboratory, University of Maryland Center for Environmental Science, Box 775 / 2020 Horns Point Road, Cambridge, Maryland 21613, USA.

ARTICLE INFO

Article history:
Received 31 October 2008
Received in revised form 31 October 2008
Accepted 1 November 2008

Keywords:
Satellite Oceanography
Ocean color
SeaWiFS
Atmospheric correction
Case 2 waters
Chlorophyll *a*
Colored Dissolved Material
Backscattering
Bio-optics

ABSTRACT

Coastal waters (Case 2) are generally more optically complex than oceanic waters and contain much higher quantities of colored detrital matter (CDM, a combination of dissolved organic matter and detrital particulates) as well as suspended sediment. Exclusion of CDM in the retrieval can lead to an overestimation of chlorophyll *a* concentration (*C*). We present a validation of a Case 2 version of the coupled spectral optimization algorithm (SOA) for simultaneous atmospheric correction and water parameter retrieval using Sea-viewing Wide Field-of-view Sensor (SeaWiFS) satellite ocean color data. Modeling of water constituents uses the Garver, Siegel and Maritorena (GSM) semi-analytic bio-optical model locally tuned for Chesapeake Bay. This includes a parameterization for CDM through its absorption spectrum.

SOA-retrieved *C* and CDM are compared with *in situ* measurements in Chesapeake Bay. Results are also compared with output from two alternate models 1) the standard algorithm (Std) and 2) the standard atmospheric correction combined with the locally tuned GSM model (StdGSM). The comparisons indicate that the SOA is a viable alternative to both given models in Chesapeake Bay. In contrast, StdGSM appears to require improvement before it can be considered for operational use in these waters. Perhaps the most important result is the high-quality of CDM retrievals with the SOA. They suggest that there is value added using the SOA method in Chesapeake waters, as the Std method does not retrieve CDM. In a companion paper we describe in detail the model implementation, and its accuracy and limitations when applied to the Chesapeake Bay.

1. Introduction

Attempts have been made to develop coupled ocean–atmosphere correction algorithms for application to ocean color data (e.g., Chomko & Gordon, 1998; Gordon et al., 1997). These algorithms use bio-optical models to relate the water-leaving reflectance ρ_w to the water's constituents and aerosol models to relate the aerosol's contribution to top-of-atmosphere reflectance ρ_t as a function of its concentration. Finding the combination of water parameter values and an aerosol model that best reproduce the measured ρ_t throughout the spectrum allows retrieval of the oceanic and atmospheric parameters simultaneously. A motivation for the coupled approach is that it does not totally rely on the spectral bands in the near infrared (NIR) to assess the aerosol's contribution to the reflectance in the visible as in the standard atmospheric correction algorithm (Gordon & Wang, 1994a). In the presence of absorbing aerosols the Gordon and Wang technique can fail because aerosol absorption cannot be assessed on the basis of NIR reflectances alone (Gordon, 1997), an important factor in coastal waters where aerosols of this type can be expected to exist.

Earlier coupled ocean–atmosphere algorithms (e.g. Chomko & Gordon, 1998, 2001; Gordon et al., 1997; Moulin et al., 2001) used the Gordon et al. (1988) two-parameter radiance model to provide the oceanic reflectance. The two-parameter model expresses ρ_w as a function of the pigment concentration P and a scattering parameter b_0. Recent ρ_w models allow for retrieval of particulate backscatter and the absorption by colored detrital materials (CDM, the sum of the absorption by dissolved organic matter and by detrital particles) in addition to the chlorophyll *a* concentration *C* (Carder et al., 1999; Garver & Siegel, 1997). Chomko et al. (2003) employed the GSM model (Garver & Siegel, 1997; Maritorena et al., 2002) in a coupled spectral optimization algorithm (SOA) to successfully retrieve both CDM and *C* in Case 1 waters of the Middle Atlantic Bight (MAB).

Of interest here is the extension of this approach to 'Case 2' waters. In contrast to 'Case 1' waters (Gordon & Morel, 1983), for which the water's optical properties vary mostly with *C*, in Case 2 waters the optical properties are also strongly influenced by suspended sediment, river runoff, etc. These waters often contain large quantities of dissolved organic material that influence ρ_t in a manner similar to absorbing aerosols. The assumption that $\rho_w(765)$ and $\rho_w(865)\approx 0$ is also often invalid (due to suspended sediment or high concentrations of

DOI of original article: 10.1016/j.rse.2008.11.001.
* Corresponding author.
E-mail addresses: c.kuchinke@miami.edu (C.P. Kuchinke), gordon@physics.miami.edu (H.R. Gordon).

0034-4257/$ – see front matter © 2008 Elsevier Inc. All rights reserved.
doi:10.1016/j.rse.2008.11.002

phytoplankton pigment and detrital particles), hence there are no bands for which aerosol effects are independent of water leaving radiance. Attempts have been made to correct for this NIR assumption in several studies using the Gordon and Wang (1994a) atmospheric correction (e.g. Arnone et al., 1998; Ruddick et al., 2000; Siegel et al., 2000). Most recently, a companion paper to this study presents a Case 2 modified version of the SOA (Kuchinke et al., 2009). This latter study highlighted the dependence of optimization models to both the error and magnitude of the bio-optical coefficients, an important consideration in Case 2 waters where regional and seasonal variability in optical properties results from differences in the sources of suspended material and CDM in different regions. Thus, there can be no 'universal' Case 2 bio-optical parameterization as, e.g., the OC4v4 (O'Reilly et al., 1998) algorithm for Case 1 waters. The Case 2 parameterizations are expected to be site specific, i.e., investigators wishing to use satellite imagery for a specific Case 2 area likely will have to develop a bio-optical parameterization that applies specifically to that area.

This study follows on from the Case 2 version of the SOA describing its implementation, accuracy and limitations in both Chesapeake Bay and Middle Atlantic Bight example bio-optical regions (Kuchinke et al., 2009). Here we compare the SOA with contemporaneous station measurements of *C* and CDM conducted by Magnuson et al. (2004), and with two other ocean color retrieval models in Chesapeake Bay: the standard atmospheric correction algorithm (Gordon & Wang, 1994a) with water properties derived using OC4v4 (Std); and an alternate model which combines the standard atmospheric correction with the GSM model in place of OC4v4 (StdGSM). These processing methods are all currently incorporated into the SeaWiFS Data Analysis System (SeaDAS) software package as options for processing in the Multi-Sensor Level-1 to Level-2 code. The comparison is undertaken using data obtained from the Sea-viewing Wide Field-of-view Sensor (SeaWiFS) on board the SeaStar polar orbiting satellite, and both the SOA and StdGSM are tuned based on the field work of Magnuson et al. (2004), Harding et al. (2004) and Tzortziou et al. (2006). The intention is to assess the performance and limitations of each of the models in the Chesapeake Bay region with possible inference to other regions with similar bio-optical properties.

We begin by describing the structure of the aerosol and water (bio-optical) reflectance models used in the SOA code. Then we briefly sketch how the optimization is achieved. Next, we introduce the *in situ* data used for both selecting the parameters of the bio-optical model that are specific to various portions of the Chesapeake Bay and for validation of the SOA-derived products. Finally, we compare retrievals made with all three processing methods with contemporaneous *in situ* data and provide some concluding remarks.

2. Aerosol and water models

At visible and NIR wavelengths λ, the total reflectance $\rho_t(\lambda)$ of the ocean–atmosphere system can be expressed as

$$\rho_t(\lambda) = \rho_r(\lambda) + \rho_A(\lambda) + t_v(\lambda)t_s(\lambda)\rho_w(\lambda) \quad (1)$$

where $\rho_r(\lambda)$ is the molecular Rayleigh scattering contribution, $\rho_A(\lambda)$ is the aerosol contribution in the presence of Rayleigh scattering, and $\rho_w(\lambda)$ is the water-leaving reflectance. The atmospheric diffuse transmittances $t_s(\lambda)$ and $t_v(\lambda)$ are from the sun to the sea surface and sensor to the sea surface, respectively. The atmospheric contribution $\rho_r(\lambda)+\rho_A(\lambda)$ includes light scattered in the atmosphere and specularly reflected from the sea surface.

2.1. The SOA atmospheric model

Mie scattering theory was used to generate aerosol optical properties given the complex index of refraction $m = m_r - im_i$, with particles distributed according to a Junge power law (see Chomko and Gordon (1998) and Kuchinke et al. (2009) for its description). Specifically, two values of m_r (1.33, 1.5), six values of m_i (0, 0.001, 0.003, 0.010, 0.030, 0.040) and six values of size distribution parameter ν (2.0 to 4.5 in steps of 0.5) were used to produce a total of 72 aerosol models, each with a specific phase function, extinction coefficient $c(\lambda)$ and single scattering albedo ω_0.

The results were used in a 2-layer radiative transfer program that computed the reflectance for a Rayleigh/aerosol atmosphere with the aerosol uniformly mixed from the surface up to 2 km to give the total atmospheric reflectance $\rho_r(\lambda)+\rho_A(\lambda)$, all as a function of the aerosol optical depth at 865 nm, $\tau(865)$. We assume that the atmosphere is bounded by a flat Fresnel reflecting ocean that absorbs all photons penetrating the surface. Subtraction of $\rho_r(\lambda)$ from the total atmospheric reflectance thus gives $\rho_A(\lambda)$ as a function of $\tau(\lambda)$, fit to a quartic expression for each geometry. The information from the quartic expression and 72 aerosol models is subsequently stored as look-up tables for use by SOA.

For the diffuse transmittance we use the same assumption as the standard algorithm, i.e., that the upwelling radiance beneath the water surface is uniform, such that

$$t_v(\theta_s, \theta_v, \phi, \lambda) \rightarrow t^*(\theta_v, \lambda) \text{ and } t_s(\theta_s, \theta_v, \phi, \lambda) \rightarrow t^*(\theta_s, \lambda).$$

Where θ_s, θ_v, and ϕ are the sun, viewing and azimuth polar angles respectively. The computed diffuse transmittance coefficients $A(\theta,\lambda)$, $B(\theta,\lambda)$ (Yang & Gordon, 1997) are also stored in the same look-up tables (for each model) where

$$t^*(\theta, \lambda) = A(\theta, \lambda) \exp\left[-B(\theta, \lambda)\tau(\lambda)\right], \quad (2)$$

and θ is either the viewing or the solar zenith angle. SOA interpolates throughout the range of parameters to essentially give a continuum of models. This is described in detail in Kuchinke et al. (2009).

2.2. The SOA bio-optical model

The water-leaving reflectance (ρ_w) is provided as a function of the total absorption (a) and backscattering (b_b) coefficients (Gordon et al., 1988). The spectral absorption and backscattering coefficients are further separated into the constituent components plus that of water:

$$\begin{aligned} a(\lambda) &= a_w(\lambda) + a_{ph}(\lambda) + a_{CDM}(\lambda) \\ a_{CDM}(\lambda) &= a_{CDOM}(\lambda) + a_{dp}(\lambda) \\ b_b(\lambda) &= b_{bw}(\lambda) + b_{bp}(\lambda) \\ a_{nw}(\lambda) &= +a(\lambda) - a_w(\lambda), \end{aligned} \quad (3)$$

where the subscripts 'w', 'ph', 'CDM', 'CDOM', 'dp' and 'nw' refer to water, phytoplankton, colored detrital material, colored dissolved organic matter, detrital particles, and non-water, respectively. Values of $a_w(\lambda)$ and $b_{bw}(\lambda)$ are known constants (Morel, 1974; Pope & Fry, 1997). The absorption due to detrital particles and colored dissolved organic matter, are combined (into CMD) due to their similar spectral signatures. In the GSM model (Garver & Siegel, 1997; Maritorena et al., 2002) all of the optical properties are modeled by three parameters: (1) the absorption coefficient of colored detrital material at 443 nm ($a_{CDM}(443)$); (2) the chlorophyll *a* concentration *C*, and (3) the backscattering coefficient of particulate material at 443 nm ($b_{bp}(443)$). Specifically,

$$\begin{aligned} a_{ph}(\lambda) &= C\, a^*_{ph}(\lambda), \\ a_{CDM}(\lambda) &= a_{CDM}(443)\exp(-S_{CDM}(\lambda - 443)), \\ b_{bp}(\lambda) &= b_{bp}(443)(443/\lambda)^{\eta}, \end{aligned} \quad (4)$$

where $a^*_{ph}(\lambda)$ is the chlorophyll *a* specific absorption coefficient spectrum for phytoplankton, S_{CDM} is the CDM spectral shape parameter and η parameterizes the spectral variation of the particulate backscattering. The quantities a^*_{ph}, S_{CDM} and η are chosen beforehand,

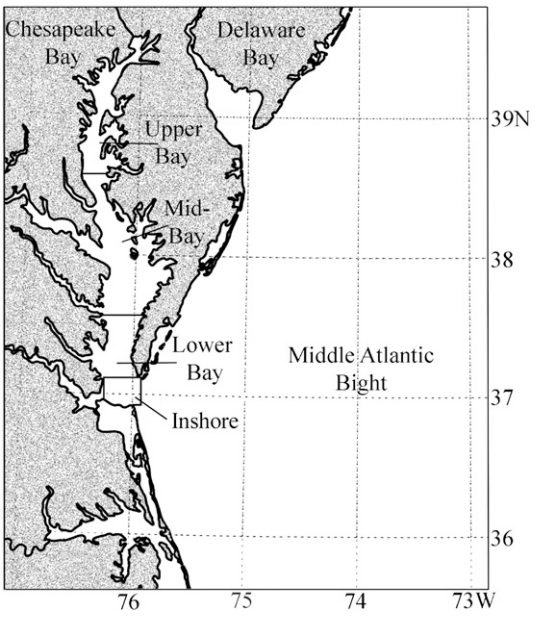

Fig. 1. Chesapeake Bay is divided into four bio-optical regions for determination of $a^*_{ph}(\lambda)$ and S_{CDM} (from Magnuson et al., 2004).

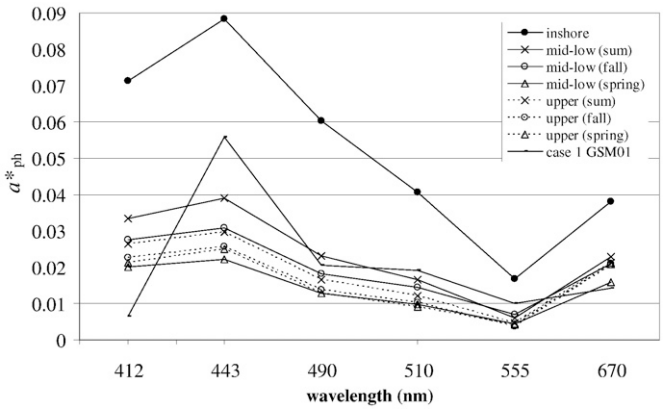

Fig. 2. Quantity $a^*_{ph}(\lambda)$ used in GSM-CB. All data from Magnuson et al. (2004) except for GSM01 (Case 1 GSM) taken from Maritorena et al. (2002).

thus the GSM water reflectance model can be represented as

$$\rho'_w(\lambda) = \rho'_w(\lambda, C, a_{CDM}(443), b_{bp}(443)), \tag{5}$$

where $\rho'_w(\lambda)$ is assumed to be independent of sun or viewing geometry (as in the computation of t^*). Henceforth, a primed symbol indicates a quantity is modeled, as in Eq. (5).

3. The Case 2 spectral optimization algorithm

SOA is operated in the SeaDAS environment for reprocessing 5.1 (2005). Quantity $\rho_t(\lambda)$ is calibrated using the current calibration curve and the spectral gains assume vicarious calibration with Gordon and Wang (1994a). Quantity $\rho_t(\lambda)$ is subsequently corrected for whitecap radiance (Gordon & Wang, 1994b), O_3 absorption, and a sun glint mask is applied. No polarization correction is used. The pressure-corrected Rayleigh contribution $\rho_r(\lambda)$ computed in SeaDAS is then subtracted from $\rho_t(\lambda)$ to give the expression $\rho_{Aw}(\lambda)$ in Eq. (6).

$$\begin{aligned}\rho_{Aw}(\theta_s, \theta_v, \phi, \lambda, \text{measured}) \equiv & \rho_A(\theta_s, \theta_v, \phi, \lambda) \\ & + t_v(\theta_s, \theta_v, \phi, \lambda) t_s(\theta_s, \theta_v, \phi, \lambda) \rho_w(\lambda)\end{aligned} \tag{6}$$

Here $\rho_t(765)$ includes O_2 absorption effects. Therefore $\rho_r(765)$ is adjusted in this step to include Rayleigh dependent O_2 absorption. Resultant $\rho_{Aw}(765)$ is then corrected to remove aerosol dependent O_2 absorption (Ding & Gordon, 1995).

The modeled counterpart of Eq. (6) can be expressed as

$$\begin{aligned}&\rho'_{Aw}(\theta_s, \theta_v, \phi, \lambda_i, m_r, m_i, \nu, \tau(865), C, a_{CDM}(443), b_{bp}(443)) \\ &\quad \equiv \rho'_A(\theta_s, \theta_v, \phi, \lambda_i, m_r, m_i, \nu, \tau(865)) + t^{*\prime}_v(\theta_v, \lambda_i, m_r, m_i, \nu, \tau(865)) \\ &\quad \times t^{*\prime}_s(\theta_s, \lambda_i, m_r, m_i, \nu, \tau(865)) \times \rho'_w(\lambda, C, a_{CDM}(443), b_{bp}(443))\end{aligned} \tag{7}$$

The estimation of parameters in Eq. (7) is achieved by spectral optimization. The procedure is undertaken as two interdependent steps. We first estimate ν and $\tau(865)$ from an exact fit to $\rho_{Aw}(NIR)$ at each gridded m_r, m_i described in Section 2.1, assuming $\rho_w(NIR)=0$, where NIR denotes the bands 765 nm and 865 nm. This results in 12 values ν and $\tau(865)$ for which functions $\nu(m_r,m_i)$ and $\tau(\lambda,m_r,m_i)$ are established by interpolation (Kuchinke et al., 2009). The minimization of the quantity in Eq. (7) is then carried out using the six visible SeaWiFS bands to estimate five parameters C, $a_{CDM}(443)$, $b_{bp}(443)$, m_r and m_i, constrained by the $\nu(m_r,m_i)$ and $\tau(\lambda,m_r,m_i)$ relationships:

$$\begin{aligned}&\sum_{\lambda_{VIS}} \{\rho'_{Aw}(\theta_s, \theta_v, \phi, \lambda_{VIS}, m_r, m_i, C, a_{CDM}(443), b_{bp}(443)) \\ &\quad - \rho_{Aw}(\theta_s, \theta_v, \phi, \lambda_{VIS}, \text{measured})\}^2\end{aligned} \tag{8}$$

In effect, all seven parameters (C, $a_{CDM}(443)$, $b_{bp}(443)$, ν, $\tau(865)$, m_r and m_i) are optimized using the eight spectral bands of SeaWiFS and the constraint that $\rho'_{Aw}=\rho_{Aw}$ in the NIR, i.e. the whole scheme provides aerosol and ocean parameters simultaneously.

The accuracy of the algorithm is dependent on several sources. Examples are the SeaWiFS digitization and noise, and the sensor calibration. The optimization mechanics and interpolations are believed to contain relatively low error. Larger errors are expected from the model parameterizations, such as the aerosol particle size distributions and bio-optical coefficients (Chomko & Gordon, 1998; Maritorena et al., 2002; Kuchinke et al., 2009) and therefore define the accuracy limits of the analysis.

The spectral optimization also takes into account the contribution to ρ_{Aw} of ρ_w in the NIR in Chesapeake Bay. Both Gordon and Wang (1994a) and Chomko et al. (2003) assume that $\rho_{Aw}(NIR)=\rho_A(NIR)$ in the atmospheric correction in Case 1 waters. In Chesapeake Bay NIR water leaving reflectance is non-zero as a result of backscatter from phytoplankton pigment and detritus (Siegel et al., 2000). To account for this we iterate SOA in the following manner. The algorithm assumes Case 1 waters i.e., $\rho'_A(NIR)=\rho'_{Aw}(NIR)$ to determine an initial estimate of $\nu(m_r,m_i)$ and $\tau(NIR,m_r,m_i)$. Estimates of $A(NIR,\theta,m_r,m_i)$ and $B(NIR,\theta,m_r,m_i)$ provide an initial estimate of $t^*(NIR,m_r,m_i)$ from Eq. (2). Subsequent operation of the quantity in Eq. (8) provides estimates of C, $a_{CDM}(443)$ and $b_{bp}(443)$ from which an estimate of $\rho'_w(NIR)$ is obtained. Ignoring m_r,m_i dependency for brevity, the estimate

Table 1
Summary of mean in situ CDM properties for the Chesapeake Bay data set used in Magnuson et al. (2004) and Harding et al. (2004)

Region	$a_{CDOM}(443)$	$a_{dp}(443)$	$\frac{a_{CDOM}}{(a_{CDOM}+a_{dp})}$	S_{CDOM}	S_{dp}	S_{CDM}
Upper	0.539	0.857	0.386	0.0160	0.0103	0.01218
Middle	0.368	0.308	0.544	0.0162	0.0123	0.01385
Lower	0.284	0.230	0.552	0.0163	0.0125	0.01330
Inshore	0.168	0.162	0.509	0.0161	0.0115	0.01236

S_{CDOM} and S_{dp} refer to the spectral slope of colored dissolved organic matter and detrital particles respectively. All other quantities are described in Section 2.2.

Table 2
Summary of cruises and corresponding SeaWiFS HRPT scenes

Cruise	Start date	End date	Image date	Parameter examined
ties9802bp	18-Jul-98	25-Jul-98	22-Jul-98	–, a_{CDM}
ties9802	04-Aug-98	12-Aug-98	11-Aug-98	*C*, a_{CDM}
ties9902	26-Jun-99	30-Jun-99	26-Jun-99	*C*, a_{CDM}
ties0003	17-Oct-00	21-Oct-00	19-Oct-00	–, a_{CDM}
ties0003	17-Oct-00	21-Oct-00	21-Oct-00	–, a_{CDM}
bio0103	02-Oct-01	06-Oct-01	3-Oct-01	*C*, a_{CDM}

The last column indicates the parameters examined in each match up.

of $t_v^* t_s^* \rho'_w$ (NIR) is then subtracted from the total reflectance i.e.,

$$\rho_{Aw}(\mathrm{NIR}) = \rho_t(\mathrm{NIR}) - \rho_r(\mathrm{NIR}) - t_v^* t_s^*(\mathrm{NIR}) \rho'_W(\mathrm{NIR}) \quad (10)$$

and the updated ρ_{Aw}(NIR) is used to initiate a new optimization, i.e., improved estimates of $\nu(m_r, m_i)$ and $\tau(m_r, m_i)$ and subsequent calculation of new water parameters. The procedure iterates until the change in ρ_{Aw}(NIR) from one iteration to the next is very small. The Case 2 manipulation increases processing times such that SOA is an order of magnitude slower than the standard algorithm in CB.

4. Bio-optical validation data for the Chesapeake Bay

4.1. Regional tuning of bio-optical model

The GSM model has been tuned for global Case 1 waters (Maritorena et al., 2002) and is referred to as GSM01. Chesapeake Bay (CB) waters are strongly affected by inputs of CDOM and detrital particles from the Susquehanna River and other tributaries. This results in strong spatial gradients of a_{CDOM} and a_{dp} from CB out to the MAB. Variability of a_{ph} in CB is also large, a result of seasonal variation in freshwater flow from its tributaries (Gallegos et al., 2005). For example, diatoms and flagellates dominate in spring and summer respectively. This warrants the need for a development of a site-

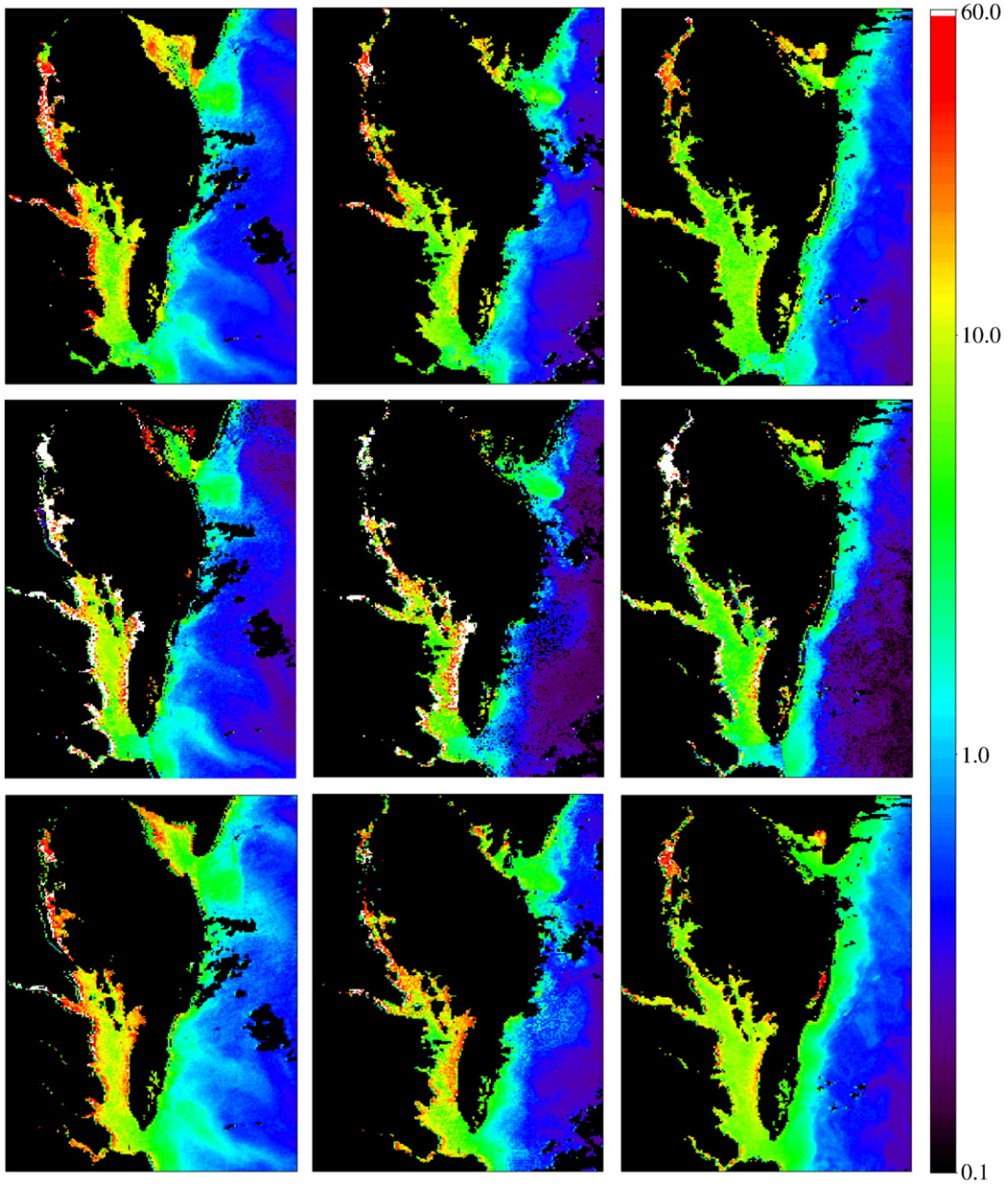

Fig. 3. Model comparison of chlorophyll *a* concentration *C* (mg m^{-3}) from SeaWiFS and for Chesapeake Bay. Columns are (l–r) 22 Jul 1998, 11 Aug 1998 and 26 Jun 1999. Rows (t–b) are SOA, StdGSM and Std models. CB bio-optical coefficients from Magnuson et al. (2004) are included in SOA and StdGSM.

specific version of GSM, namely GSM-CB. For this task we require local knowledge of the bio-optical coefficients $a^*_{ph}(\lambda)$, S_{CDM} and η in Eq. (4).

Cruises were undertaken in April, July, August and October 1996 to 2004 and consisted of approximately 10 to 20 chlorophyll *a* stations and 2 to 10 CDM stations per cruise. Some cruises contained incomplete data sets. Quality control applied to *in situ C* during the selection phase included exclusion of stations external to the bay, reducing the sample size by approximately 10%. We used both fluorometric and HPLC data for *C*, following the approaches of Garver and Siegel (1997) and Magnuson et al. (2004). Fluorometric *C* was determined on 90% acetone extracts of sample filters from additional stations for which HPLC analyses were not performed, constituting approximately 20% of the samples. Pure chlorophyll *a* standards (Sigma-Aldrich Co.) were used to calibrate fluorometric readings. For HPLC, NASA protocol required inclusion of divinyl chlorophyll *a*, monovinyl chlorophyll *a* and chlophyllide *a*. Divinyl chlorophyll *a* was found in less than 2% of all collected HPLC samples. No extra quality control was applied to CDM data due to its low initial sample size. Measurements of a_{CDOM}, a_{dp} and a_{ph} were referenced to 443 nm for further use.

To increase spatial accuracy, Magnuson et al. (2004) classified CB waters into several regional zones with boundaries loosely distinguished by differences in the attenuation coefficient of downwelling irradiance K_d between water masses (Fig. 1). The *upper* bay is defined as the CB region north of 38.60°N, the *middle* bay between 38.60°N and 37.60°N, the *lower* bay between 37.60°N and 37.11°N and the mouth or *inshore* defined as the region between 37.11°N and 36.90°N and 75.90°W and 76.25°W. An optimization procedure using a comprehensive CB data set of inherent and apparent optical properties from 1996 to 2004 determined the best values of bulk optical properties $a^*_{ph}(\lambda)$ and S_{CDM} for retrieving the two unknowns — *C*, and $a_{CDM}(443)$ (Harding et al., 2004; Magnuson et al., 2004). Analysis of mean phytoplankton pigment absorption $\langle a^*_{ph}\rangle$ from 400 to 700 nm at different times of the year was used to infer seasonal differences in the analyses.

Fig. 2 shows the results for $a^*_{ph}(\lambda)$. The *upper* bay values are low in both magnitude and seasonal divergence. In contrast the *middle* and *lower* bay regions are higher in magnitude in fall and spring and display stronger seasonal dependence. They were grouped together to form the same ensemble *mid–low* in Magnuson et al. (2004) and this study. The *inshore* station measurements were three times higher than elsewhere and always conducted along a north–south transect at the mouth of CB. Hence they fail to encapsulate any longitudinal variability. We acknowledge that the quantity a^*_{ph} contains inaccuracies due to inappropriate assumptions in the pigment analysis. The most important factors are (1) the laboratory-determined path length amplification factor β. This error is perhaps larger in CB *inshore* waters where seasonal influence of optically different offshore waters is possible, and (2) the presence of phaeophytin that is generally responsible for the largest deviations from the typical ensemble as blooms senesce, i.e., a^*_{ph} is not specific to chlorophyll *a* alone but to the total pigment ensemble. Inspection of *in situ* data in this study showed that some CB waters contained phaeophytin concentrations up to 40% of *C*.

The quantity S_{CDM} (nm^{-1}), the spectral shape parameter for a_{CDM}, was estimated from 400 to 650 nm by using a nonlinear fit with absorption spectra of measured a_{CDOM} and a_{dp} combined. Both a_{CDOM} and a_{dp} show a strong correlation with salinity in CB, both decreasing as salinity increases southwards (Harding et al., 2004 and Table 1). Statistical analysis showed that differences in *S* were significant regionally but not seasonally, with the mean values of S_{CDOM}, S_{dp} and S_{CDM} also given in Table 1. For the *upper* bay dissolved material accounts for approximately 39% of the CDM absorption. In the lower three regions the value is 50 to 55%, with the highest proportions in the *middle* and *lower* bay.

The power law exponent for spectral backscatter η describes the spectral shape of backscattering due to all particulates combined (phytoplankton, detrital particles, and suspended sediment). In the absence of sediment, this term has been shown to increase from open eutrophic to oligotrophic waters (Loisel et al., 2006). It may also

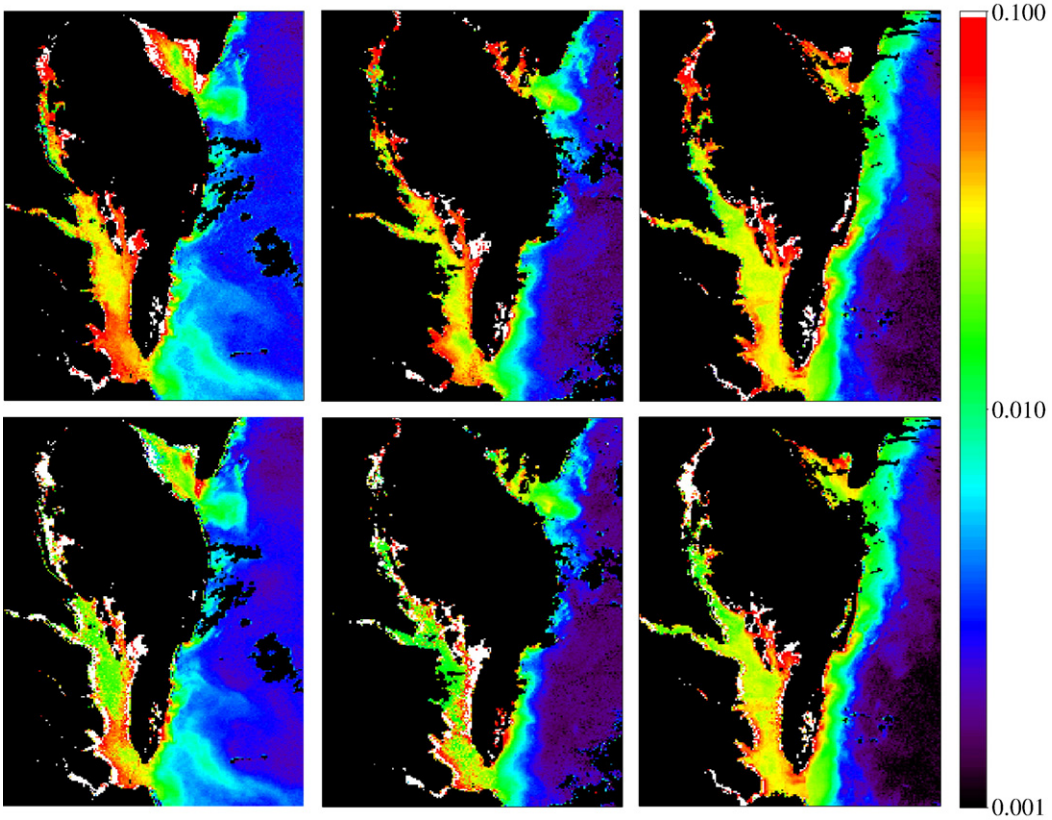

Fig. 4. Model comparison of $b_{bp}(443)$ (m^{-1}) from SeaWiFS. Columns are (l–r) 22 Jul 1998, 11 Aug 1998 and 26 Jun 1999. Rows (t–b) are SOA and StdGSM.

depend on the particulate distribution from river sources. For example, η has been shown to approximate 1.22 in Case 2 Santa Barbara waters off California whereas it approximates 1.03 in Case 1 waters (Maritorena, 2005; Maritorena et al., 2002). It is important to mention that the parameterization of sediment is not included in the GSM-CB model. It is likely that variability in suspended sediment of lithogenous or biogenous source will affect the total particulate backscattering in the *upper* bay at various times and the shape of η(sediment) may differ from η(phytoplankton+detritus).

Estimation of η was undertaken separately in this study. Backscattering coefficient information in CB is limited, but measurements have been recorded in the *middle* bay at the mouth of the Potomac River (2 samples) and *upper* bay (9 samples) at 450, 550 and 650 nm (Gallegos, 2006; Tzortziou et al., 2006). Quantity η was then derived using quadratic interpolation and the expression for b_{bp} in Eq. (4). Results for the *upper* and *middle* bay produced η=1.095 (±0.29) and 1.45 (±0.22) respectively, with the standard deviation (SD) in parentheses. Given the low number of samples in the *middle* bay, it was decided to accept 1.095 for all regions of the bay acknowledging that this value is likely to vary both spatially and seasonally. This value of η along with $a^*_{ph}(\lambda)$ and S_{CDM} from Magnuson et al. (2004) were updated to GSM-CB for further application.

Clearly, there is likely to be significant error in the values of η, $a^*_{ph}(\lambda)$ and S_{CDM} that are employed in the CB. To help understand the influence of such errors, Kuchinke et al. (2009) provide examples of the degradation in the quality of retrievals given error in the individual bio-optical parameters.

4.2. Contemporaneous SeaWiFS data

A search of the entire SeaWiFS archive of High Resolution Picture Transmission (HRPT) scenes was undertaken to evaluate the best match up with cruise data. The two primary considerations were cloud free imagery and CB satellite pixels less than 1.5 km in width. That is, a sensor zenith angle in CB<40°. A total of 16 clear sky matching scenes from 1996 to 2004 were extracted and further reduced to six after consideration for satellite sensor zenith angle and frequency of corresponding *in situ* measurements. Table 2 lists the SeaWiFS image days used in this study and their corresponding cruises. Note here that only cruise data two days either side of an image day are included in the analysis. This fact is more important to *C* aliasing, as CDM is less variable in space and time. The last column gives the parameter examined, with frequency of *in situ C* limiting the *C* match ups to just three days.

5. Model results and validation for Chesapeake Bay

The standard atmospheric correction has been coupled with the GSM-CB bio-optical model and is referred in this study as StdGSM. In this procedure values of *C*, $a_{CDM}(443)$ and $b_{bp}(443)$ are varied using GSM-CB until a best fit of normalized $\rho_w(\lambda)$ is obtained using *simplex* optimization after standard atmospheric correction. This method differs structurally from SOA; it only optimizes across all six SeaWiFS visible bands for the bio-optical model. SOA optimizes for both atmosphere and bio-optical model simultaneously.

5.1. Chlorophyll a results and validation

5.1.1. Comparison with SeaWiFS operational products

Three full resolution SeaWiFS scenes are analyzed for *C* and b_{bp} (443) in Figs. 3 and 4, respectively. The atmosphere over the MAB on these days was moderately turbid, with retrieved τ(865) between 0.08 and 0.2. The columns (l–r) in both figures correspond to 22 Jul 1998, 11 Aug 1998, and 26 Jun 1999 respectively from Table 2. The rows (t–b) in Fig. 3 correspond to *C* output (mg m^{-3}) for SOA, StdGSM and Std (standard algorithm). In Fig. 4 the rows (t–b) correspond to b_{bp}(443) for SOA and StdGSM. As a reminder Std uses the band ratio algorithm OC4v4 for *C* retrieval and hence contains no b_{bp} product. All models use the same sensor calibration and preprocessing of ρ_t–ρ_r as for SOA. GSM-CB coefficients are the same in both SOA and StdGSM and applied in CB. For illustration purposes, GSM01 coefficients are used in the MAB external to *inshore* region.

The upper limit of the *C* scale in Fig. 3 (60.0 mg m^{-3}) corresponds to the upper limit of *C* in SOA. This limit (above which we consider the procedure to have failed) corresponds to 20 to 30% of the SOA and Std retrievals in the *upper* bay for all *C* imagery. Performance of StdGSM is relatively poor in most regions, shown as the white pixels in both *C* and b_{bp} (upper limit: 0.1 m^{-1}) imagery.

Approximately 50% of the very high *C* values in the *upper* bay are believed to be due to adjacency affects. Furthermore, the possibility of high suspended sediments not parameterized in GSM-CB or OC4v4 may increase the reflectance in a manner dissimilar to phytoplankton and detritus. Temporal variability in S_{CDM} is also a significant source of error. For example, a 20% error in S_{CDM} in CB, for high *C* and CDM, was shown in Kuchinke et al. (2009) to vary the SOA *C* retrieval by at least 30% (bottom left panel of their Fig. 5a).

The coarse imagery scale for *C* conceals some of the spatial structure evident in the methods. The scale of the b_{bp} imagery divulges more of this structure. All three scenes contain a central filament of lower *C* (and hence lower b_{bp}) running north–south and higher *C* (high b_{bp}) of several km width adjacent to the coast. Model Std gives higher values than SOA adjacent to the coast on all three days. In the central areas Std remains higher than SOA but the differences are reduced. SOA and StdGSM values are actually similar for about half the pixels in this central north–south filament, with the remainder of the StdGSM pixels relatively 'noisy'.

Overall, SOA and Std structure is similar on all 3 days. Both algorithms give similar results in the *upper* bay. The SOA is 10 to 30% lower than Std in the lower three regions of the bay. SOA and StdGSM performance is markedly different across all 4 optical regions of the bay, with SOA consistently more robust (less noise) and more successful in terms of number of retrievals. This suggest that at least some of the difference between SOA and StdGSM is due to the optimization handling of GSM-CB, given that Std and StdGSM use the same atmospheric correction. To confirm this, the SOA optimization mechanics would need to replace the simplex method in StdGSM and intercompared in a similar vain to this study to see the improvement.

5.1.2. Comparison with in situ surface measurements

Pixel data from all *C* imagery in Fig. 3 is displayed in frequency histograms in Fig. 5. This method is the preferred choice for direct comparison, as temporal variability in *C* can be 20% to 30% over the course of several hours rendering an exact pixel to *in situ* comparison difficult. The frequency data are organized into 3 blocks corresponding to the 3 days 22 Jul 1998, 11 Aug 1998, and 26 Jun 1999 (t–b). Within each data block the results are column binned by CB region from *upper* to *inshore* (l–r). Data is also grouped into rows according to its source — t–b: SOA, StdGSM, Std and *in situ*. Note that no data exists for the *inshore in situ* measurements on 22 July 1998. The *x* coordinates depict log *C* in steps of 0.2 and labeled for the center of the range. For example, label 0.1 corresponds to log *C* from 0 to 0.2 (*C*=1.0 to 1.6 mg m^{-3}) and label 1.7 corresponds to log *C* from 1.6 to 1.8 (*C*=39.8 to 63.1 mg m^{-3}). Hence, the aim of the histograms is to emphasize the relative distribution of *C* in the CB. Note that model StdGSM does not constrain *C* to upper and lower boundaries in its GSM-CB optimization. Similarly, Std contains no upper limit for *C*. Therefore, we reassigned all output of both models to the upper and lower *C* boundaries in the SOA i.e., all values >60 equal 60 and all values <0.02 equal 0.02 (units in mg m^{-3}). It is worth mentioning here that most instances outside the range were in fact unrealistic values (failures). Finally, all *inshore* measurements were conducted in a relatively narrow width north–south transect at the mouth of CB. To

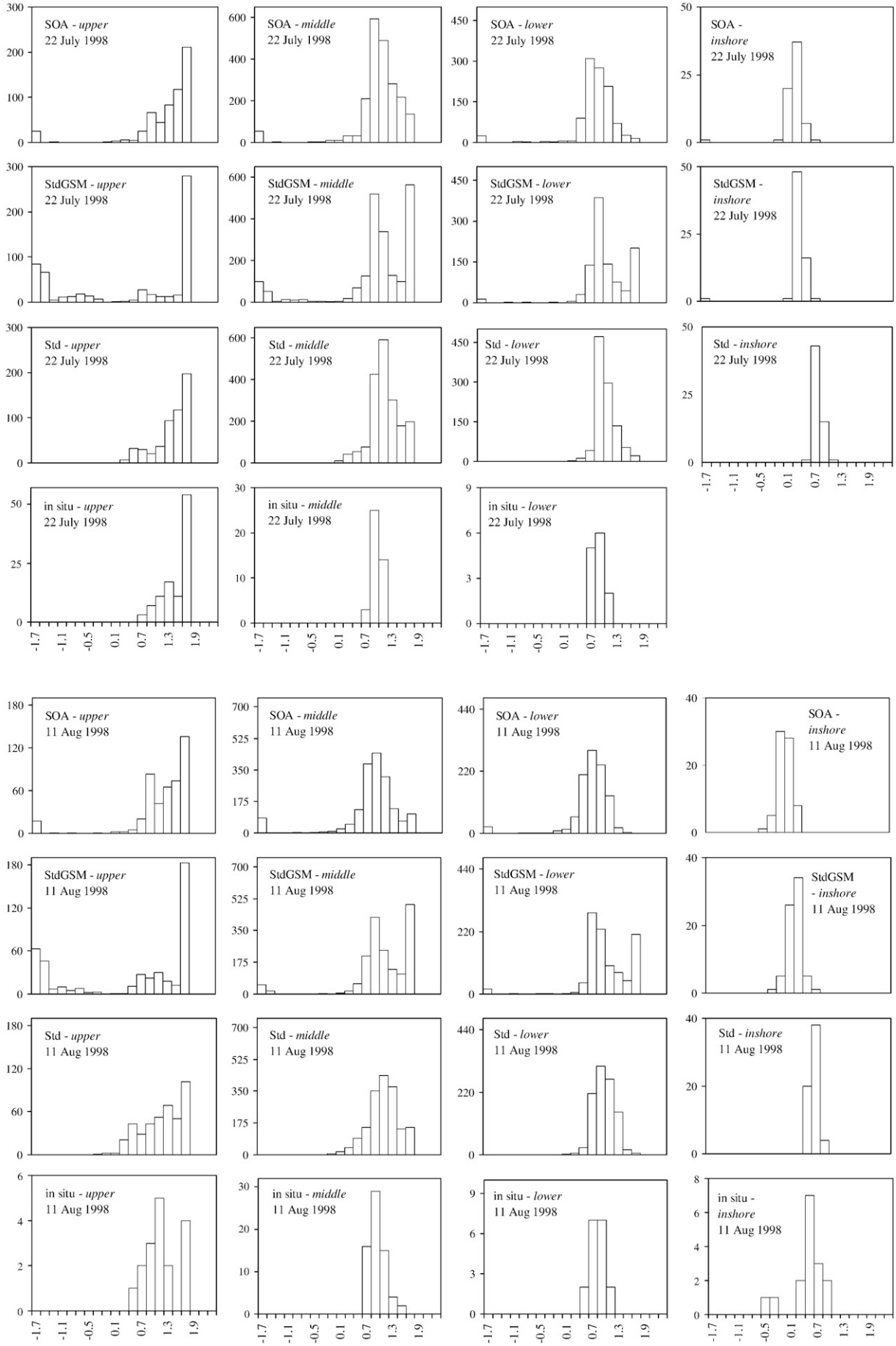
SOA - upper 22 July 1998
SOA - middle 22 July 1998
SOA - lower 22 July 1998
SOA - inshore 22 July 1998
StdGSM - upper 22 July 1998
StdGSM - middle 22 July 1998
StdGSM - lower 22 July 1998
StdGSM - inshore 22 July 1998
Std - upper 22 July 1998
Std - middle 22 July 1998
Std - lower 22 July 1998
Std - inshore 22 July 1998
in situ - upper 22 July 1998
in situ - middle 22 July 1998
in situ - lower 22 July 1998
SOA - upper 11 Aug 1998
SOA - middle 11 Aug 1998
SOA - lower 11 Aug 1998
SOA - inshore 11 Aug 1998
StdGSM - upper 11 Aug 1998
StdGSM - middle 11 Aug 1998
StdGSM - lower 11 Aug 1998
StdGSM - inshore 11 Aug 1998
Std - upper 11 Aug 1998
Std - middle 11 Aug 1998
Std - lower 11 Aug 1998
Std - inshore 11 Aug 1998
in situ - upper 11 Aug 1998
in situ - middle 11 Aug 1998
in situ - lower 11 Aug 1998
in situ - inshore 11 Aug 1998
-1.7 -1.1 -0.5 0.1 0.7 1.3 1.9

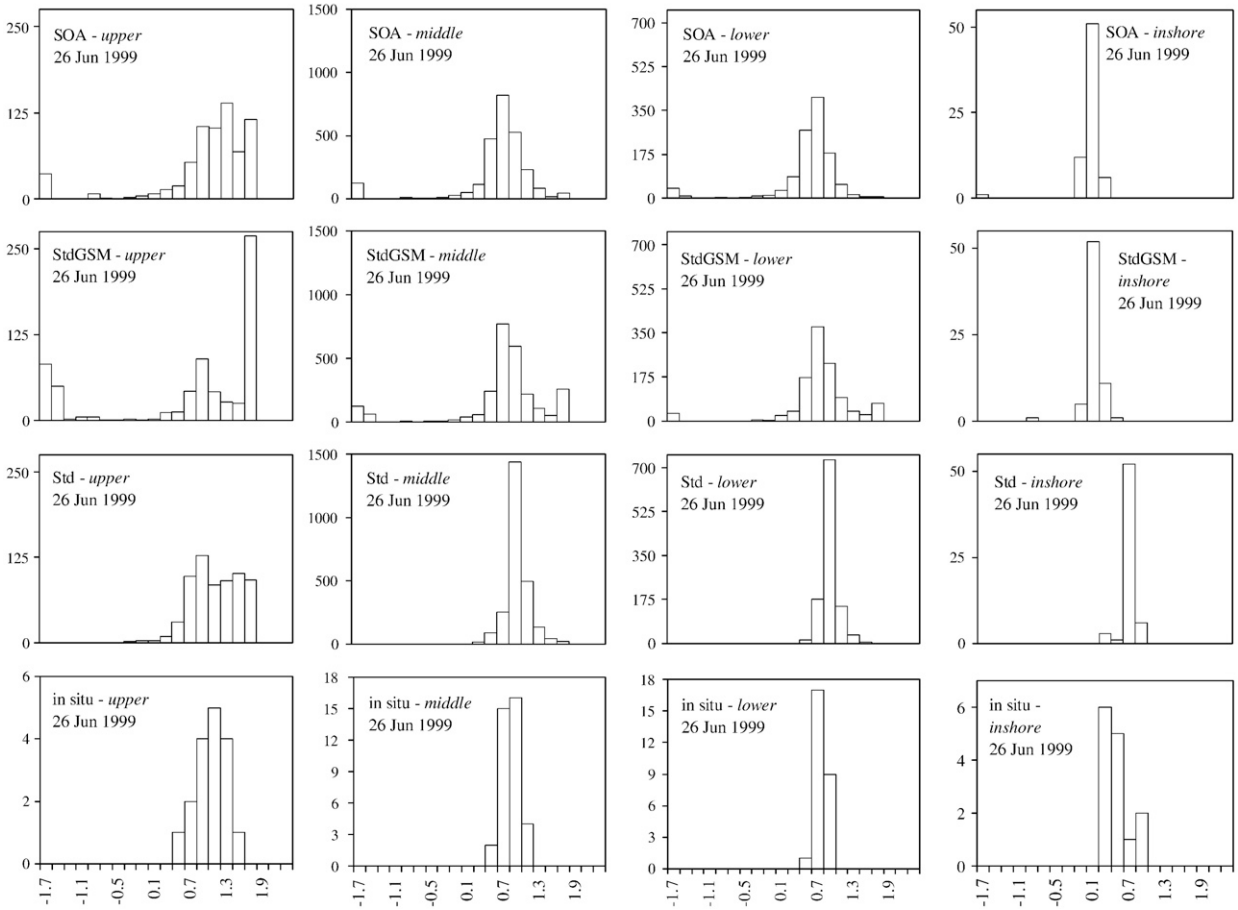

Fig. 5. Frequency (y-axis) versus log *C* (x-axis) in Chesapeake Bay. The data is divided into three large data blocks (t–b) — 22 July 1998, 11 Aug 1998 and 26 Jun 1999. In each data block, the rows (t–b) represent SOA, StdGSM, Std, and *in situ*. The columns (l–r) represent the different regions of the bay: *upper*, *middle*, *lower* and *inshore*.

coincide with this we only processed model data within 2 pixels either side of this narrow spatial swath. This effectively reduced the region's area from approximately 550±100 pixels to about 65±10, depending upon the scene.

Concentrating on the relative histogram shapes in Fig. 5, SOA and Std *C* retrievals in the *upper* bay are once again very similar to *in situ C* on all three days as discussed previously for Fig. 3. In detail, SOA and Std display very similar distributions on the first and third day with the best match up with *in situ* data on the first day. On the second day, 11 Aug 1998, the SOA is slightly improved over Std as evidenced by the two distinct peaks in both the *in situ* data and SOA. StdGSM *C* retrieval in the *upper* bay is quite poor across the same days evidenced by the large number of retrieval failures.

In the *middle* bay the peak of the SOA distribution is best aligned with the *in situ* data on all days. StdGSM is improved from the *upper* bay but still exhibits a pixel failure rate of 30%. The Std distribution is shifted to higher values of *C* on all three days.

SOA and StdGSM have the same distribution on all three days if the failures are removed from StdGSM. These distributions have a similar peak but wider spread compared to the *in situ* distributions.

In the *lower* bay, the distribution of all three algorithms is similar. However, the SOA is shifted to slightly lower values relative to *in situ*. In contrast Std is shifted to slightly higher values, particularly on the last two days 11 Aug 1998 and 26 Jun 1999.

The last day 26 Jun 1999 is characterized by very strong agreement between SOA, StdGSM and *in situ*. StdGSM contains about 20% failures on all three days.

For the *inshore* region, SOA and StdGSM have strong agreement on all days. Std values are considerably higher compared to the alternate two models. On the days for which observations are given (11 Aug 1998 and 26 Jun 1999) the *in situ* measurements lie between the lower SOA and StdGSM and higher Std.

To summarize the distributions, SOA and Std are similar in the *upper* bay. However, in the *middle* and *lower* bay the SOA distribution provides the better match up with the *in situ* data. The Std values appear overestimated for several of the cases. Interestingly, SOA and StdGSM have similar distribution shapes if the failures are removed from StdGSM. SOA and StdGSM underestimate in *inshore*, while Std overestimates. In terms of retrieval success, SOA and Std contain 20–30% failure in the *upper* bay but robust performance in the lower three regions with relatively low number of failures. StdGSM contains, on average, 40–50% failure in the *upper* bay and 15–20% failure in *middle* and *lower* bay. Performance in *inshore* is reasonable with low failures. As discussed in the previous section, temporal variability in $a^*_{\mathrm{ph}}(\lambda)$, S_{CDM} and η are significant sources of error, as well as suspended sediments not included in the model.

Comparison of the mean, median and standard deviation values are presented in Table 3 for *C* derived from each model and *in situ* data in each CB region. It is noted that the actual spread in the retrievals comprises both error in the analysis and natural spread in the *C* spatial structure.

Mean results in the *upper* bay are mixed but do support the use of SOA. It appears to perform at least as well if not better than Std or

Table 3
Summary of *C* mean, median and standard deviation (SD) for all pixels in each region of Chesapeake Bay presented in Fig. 5

Date	Class	# Pixels	Upper Bay			# Pixels	Middle Bay		
			Mean	Median	SD		Mean	Median	SD
22 July 98	SOA	588	37.3	40.6	22.9	2070	16.5	9.9	16.7
	StdGSM		34.0	60.0	28.2		23.8	11.1	22.8
	Std		29.1	25.8	19.8		18.0	12.4	14.8
	In situ	87	48.0	29.6	58.0	42	9.1	9.0	2.0
11 Aug 98	SOA	449	32.9	25.2	23.5	1751	11.7	7.5	13.2
	StdGSM		31.8	28.4	27.4		24.3	11.8	22.5
	Std		39.2	15.6	82.7		18.5	12.5	30.9
	In situ	17	20.4	11.4	19.4	66	9.8	8.6	5.3
26 Jun 99	SOA	666	21.1	15.2	18.8	2550	7.0	5.1	8.2
	StdGSM		32.6	29.8	26.5		12.6	7.3	16.9
	Std		23.3	11.5	39.1		9.8	8.1	7.0
	In situ	17	12.9	11.6	7.6	37	6.9	6.6	2.3
Date	Class	# Pixels	Lower Bay			# Pixels	Inshore		
			Mean	Median	SD		Mean	Median	SD
22 July 98	SOA	1036	9.4	7.1	8.3	67	1.9	1.8	0.6
	StdGSM		19.5	9.1	20.1		2.3	2.2	0.6
	Std		12.8	9.9	8.4		6.0	5.8	1.2
	In situ	13	8.2	7.9	2.1	–	–	–	–
11 Aug 98	SOA	1014	6.3	5.2	4.1	72	1.1	1.0	0.4
	StdGSM		19.6	8.2	20.9		1.7	1.6	0.7
	Std		10.9	9.0	7.7		5.7	5.0	3.2
	In situ	18	6.8	6.8	2.6	12	3.9	4.4	2.2
26 Jun 99	SOA	1107	5.3	4.4	5.1	70	1.3	1.2	0.3
	StdGSM		10.2	5.6	14.0		1.4	1.4	0.4
	Std		8.4	7.5	3.5		5.4	5.4	1.4
	In situ	27	5.8	6.0	1.1	14	3.5	3.2	1.5

Data is given for the three models SOA, StdGSM and Std as well as *in situ* data. Note that *inshore* corresponds to a narrow width north–south transect at the mouth of Chesapeake Bay in accordance with the *in situ* data.

StdGSM. The spread in Std results is quite high relative to the other two models, perhaps indicating that GSM gives improved results in areas dominated by high *C*, CDM and possible sediments, an artifact of OC4v4 apportioning all absorption to a_{ph}, or at least a constant fraction of a_{nw} to a_{ph}.

Mean results for the *middle* and *lower* bay show stronger support for the use of SOA versus the other two models for most of the data. Mean retrievals for StdGSM and Std appear to overestimate *C*, however some improvement is seen in Std on the third presented day, 26 Jun 1999. In both *middle* and *lower* CB the spread in StdGSM retrievals appears unrealistically high, indicating possible error.

Results are different for the *inshore* region. We emphasize that satellite retrievals here were confined to the very thin transect for which observations were taken in order to better harness the low number of observations. It does appear that Std overestimates the *in situ* data while SOA and StdGSM underestimate for the two latter days for which observations are given. One possible explanation here is that once again OC4v4 cannot account for waters containing high CDM, while the GSM-CB coefficients may also be in error. This is discussed further in the next section.

5.2. CDM results and validation

Three full resolution SeaWiFS scenes are presented for $a_{CDM}(443)$ on 22 July 1998, 11 Aug 1998 and 26 Jun 1999 in Fig. 6(l–r). The rows (t–b) correspond to SOA and StdGSM. Some artificial linear features are evident due to a non-smooth transition in a^*_{ph} between CB regions; for example, portions of the near-horizontal boundary between *lower* and *inshore* regions.

The *upper* bay mean $a_{CDM}(443)$ from the observations in Table 1 is approximately 1.4 m^{-1}. The upper boundary for $a_{CDM}(443)$ in SOA is 1.3 m^{-1}. This is the maximum value that the SOA can retrieve, and such retrieval is considered "SOA failure" because it suggests that a higher value is desired by the optimization procedure.

For the CB *upper* bay region, SOA failure is of the order of 10 to 20%. StdGSM $a_{CDM}(443)$ failure is approximately 95%. These are "true" failures in the sense that most of the retrievals are unnaturally high compared to the observations. Results for the *middle*, *lower* and *inshore* regions are dramatically improved for SOA but not for StdGSM on two of the three days (22 Jul 1998 and 11 Aug 1998). These two days correspond to relatively low SOA-retrieved aerosol optical depth over CB compared to 26 Jun 1999. Paradoxically, this suggests StdGSM has difficulty when total $\rho_{Aw}(\lambda)$ is low. In all regions of CB, the maximum value for most red pixels in SOA is in the range 0.7 to 0.85 m^{-1}.

An *in situ* comparison was undertaken by extraction of $a_{CDM}(443)$ measurements from the cruise date sets (Table 2). Both SOA and *in situ* measurements were averaged in each region of the bay and the ratio comparisons given in column 5 of Table 4. The *upper* bay values range from 0.70 to 1.02, *middle* from 0.85 to 1.14, *lower* from 0.88 to 1.32 and *inshore* from 0.36 to 1.01. The four lowest values of SOA relative to the *in situ* are presented in bold and all correspond to the *inshore* region of CB. This is in accordance with the SOA-*C inshore* match ups in the previous section which were also underestimated. The results here at least show that the SOA $a_{CDM}(443)$ retrieval appears robust for the *upper*, *middle* and *lower* regions of CB.

Table 4 also gives the coefficient of variation (CV) of the ratio, defined as SD/mean. The approximate 20 to 40% spread in the data is comprised of real variability in CDM structure. However, the *inshore* region again is anomalous as seen in the consistently high CV difference between SOA and *in situ*.

The quantity a_{CDM}/a_{nw} at 443 nm provides a relative measure of CDM to total constituents CDM+ph in the surface water column. Ratio $[SOA(a_{CDM}/a_{nw})/in\ situ(a_{CDM}/a_{nw})]$ in the last column of Table 4 shows that the bio-optically tuned SOA does a reasonable job at partitioning the relative CDM and phytoplankton pigment absorption components, with the exception of *inshore* as discussed above.

An assessment of the error sources in the retrieved a_{CDM} is difficult; however, several observations are helpful. As discussed earlier, adjacency effects and local suspended sediment hinder an accurate retrieval in *upper* CB. It is also likely that the proportion of $a_{CDOM}(443)$ to $a_{CDM}(443)$ may differ from the mean result in Table 1. This will result in the use of an incorrect coefficient S_{CDM} in GSM-CB and likely error (see accompanying paper Kuchinke et al. (2009) which discusses the influence of error in S_{CDM}). In the case of the *inshore* region, the main source of error is considered to be a result of the bio-optical modeling. Only 26 *inshore* measurement stations were used to derive GSM-CB *inshore* bio-optical coefficients in the Magnuson et al. (2004) study, the lowest analysis data set for all CB regions. In addition, for lack of adequate measurements, the back-scattering spectral coefficient η in *inshore*-CB was set separately using the *upper* bay estimate in this study. Seasonal bias was considered and eliminated as an error source for derivation of the *inshore* bio-optical coefficients, because two measurement stations were in spring, 19 in summer and five in autumn, while *in situ* measurements in Table 4 correspond to three days in summer and three in autumn.

In accompanying paper (Kuchinke et al., 2009), we presented SOA $a_{CDM}(443)$ retrieval performance as a function of bio-optical coefficient error. The study showed that the accuracy of $a_{CDM}(443)$ (using *lower* CB bio-optical coefficients) is reduced given an increase in the ratio of $a_{ph}(\lambda)$ to $a_{nw}(\lambda)$ (Eq. (3)). This suggests that SOA $a_{CDM}(443)$ accuracy should indeed worsen as we move from *upper* to *inshore* CB. More importantly, it was shown that if S_{CDM} is underestimated *or* overestimated by 40% then the SOA CDM retrieval is underestimated by also 20 to 40% (third row of Fig. 6a of Kuchinke et al., 2009). This would be the error required in S_{CDM} to fully

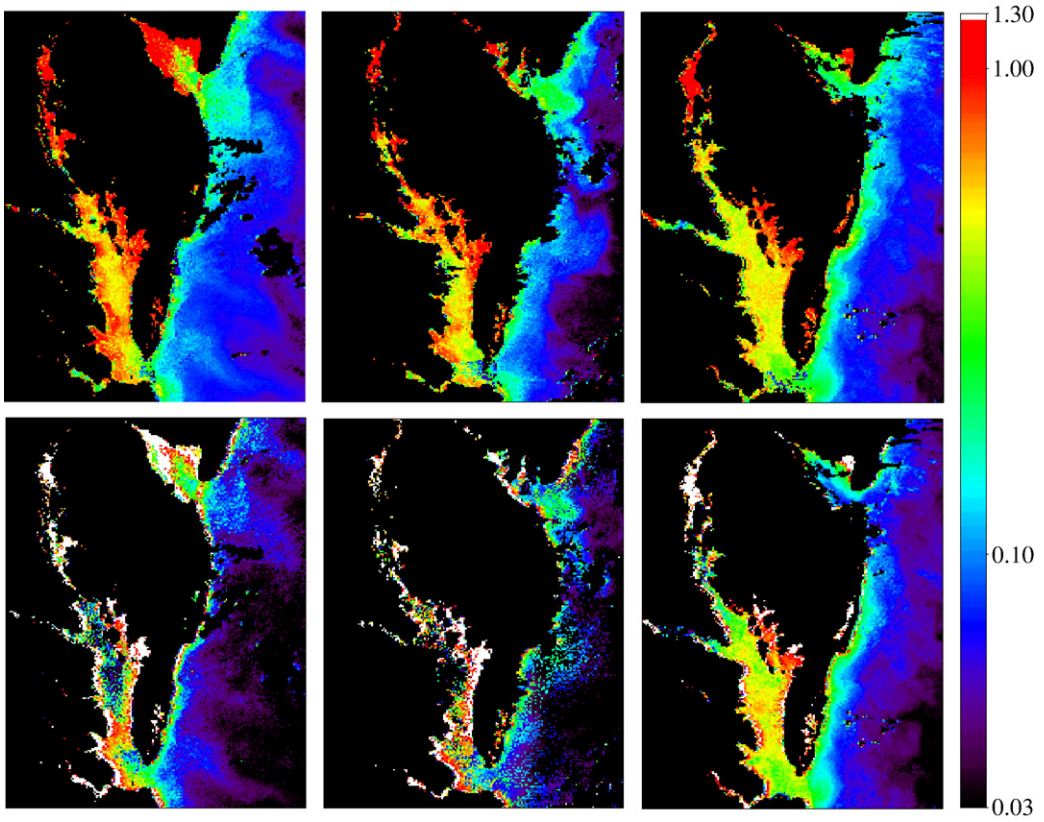

Fig. 6. Model SOA colored detrital material CDM (m^{-1}) for (l–r) 22 July 1998, 11 Aug 1998 and 26 Jun 1999 using SeaWiFS data. Rows (t–b) are SOA and StdGSM. The bio-optical model is tuned in Chesapeake Bay. The SOA-retrieved optical depth is high on 26 Jun 1999 high relative to the two other days.

explain the results shown in Table 4. It is likely that bio-optical error explains part of the error, with aliasing and SOA error likely to be present.

The low number of validation samples was also considered as a possible error source; however, inspection of *in situ* CDM indicated very low spatial variability at both diurnal and daily scales. For example, at a similar latitude and longitude, *in situ* $a_{CDM}(443)$ actually changed by less than 2 to 5% across any six hour window.

Table 4
Comparison of SOA and *in situ* $a_{CDM}(443)$, averaged for each region of Chesapeake Bay

Image	Region	# *In situ*	# Pixels	$a_{CDM}(443)$ SOA/*in situ*	CV *in situ*	CV SOA	$\frac{SOA(a_{CDM}/a_{nw})}{in\ situ\ (a_{CDM}/a_{nw})}$
22-Jul-98	Upper	7	588	0.704	0.174	0.619	0.934
11-Aug-98	Upper	3	449	0.788	0.022	0.364	0.801
	Mid	15	1753	0.850	0.255	0.449	0.874
	Inshore	6	72	**0.361**	**0.352**	**0.979**	**0.484**
26-Jun-99	Upper	4	673	0.895	0.248	0.303	1.041
	Mid	6	2562	0.891	0.193	0.456	1.017
	Inshore	6	70	**0.534**	**0.178**	**0.504**	**0.698**
19-Oct-00	Upper	4	750	1.004	0.057	0.347	0.872
	Mid	6	2786	1.136	0.099	0.310	1.059
	Lower	3	1203	1.005	0.247	0.262	1.053
	Inshore	2	70	1.013	0.181	0.599	0.597
21-Oct-00	Upper	4	876	1.020	0.057	0.334	0.812
	Mid	6	2658	0.926	0.099	0.377	1.012
	Lower	3	1119	0.882	0.247	0.261	1.017
	Inshore	2	73	**0.428**	**0.181**	**0.778**	**0.394**
3-Oct-01	Upper	4	957	0.894	0.185	0.428	0.984
	Mid	3	2816	1.140	0.126	0.402	1.079
	Lower	2	1231	1.326	0.040	0.273	1.365
	Inshore	2	72	**0.605**	**0.016**	**0.817**	**0.570**

SOA [$a_{CDM}(443)$/*in situ* $a_{CDM}(443)$] is shown in column five. Coefficient of Variation (CV)=[standard deviation/mean]. Quantity a_{nw} in the last column is $a_{CDM}+a_{ph}$ from Eq. (3). The four worst match ups are given in bold.

5.3. SOA accuracy estimation in Chesapeake Bay from synthetic data

The companion paper Kuchinke et al. (2009) produced a predictive function for estimating SOA performance by comparison of modeled $f(a,b_{bp})$ and $f(a)$ synthetic data (Eq. (11) below) with SOA retrievals given $\tau(865)=0.1$ and $u=100$.

$$f(a,b_{bp}) = \left(\frac{a_{CDM}(443)}{a_{ph}(443)+a_{CDM}(443)}\right)^2 (b_{bp}(443)u)^{-1} \quad (11)$$

Cruise measurements obtained in this study indicate that $a_{cdm}(443)/[(a_{cdm}(443)+a_{ph}(443)]$ is generally in the range 0.4 (*lower* bay) to 0.6 (*middle* bay) and >0.7 in the *upper* bay. These estimates do not account for seasonal variability. Backscattering measurements are limited in CB as discussed. However, operation of the SOA for many scenes indicates that $b_{bp}(443)$ is nearly always >0.01 m^{-1} for all regions of CB as in Fig. 4. Using this analogy, this predicts that in the *lower* bay $f(a,b_{bp})=0.16$ and 0.032 for $b_{bp}(443)=0.01$ and 0.05 respectively. From Fig. 3 in the companion paper, *C* is therefore likely to contain 20% error at reduced $b_{bp}(443)$, improving as we increase $b_{bp}(443)$. For the *upper* bay and using a very high $a_{cdm}(443)$ to $a_{cdm}(443)+a_{ph}(443)$ ratio of 0.9, $f(a,b_{bp})=0.16$ at $b_{bp}(443)=0.01$, resulting in up to 70% error in the *C* retrieval. This reduces to approximately 30% for $b_{bp}(443)=0.05$ in the same region. Similarly, in the lower bay $f(a)=0.16$ irrespective of $b_{bp}(443)$. The companion paper predicts a maximum error of 20% in the $a_{cdm}(443)$ retrieval here. In the *upper* bay, and using $a_{cdm}(443)$ to $a_{cdm}(443)+a_{ph}(443)$ ratio of 0.9, $f(a)=0.81$. This is expected to result in a very good $a_{cdm}(443)$ retrieval assuming no sediment is present.

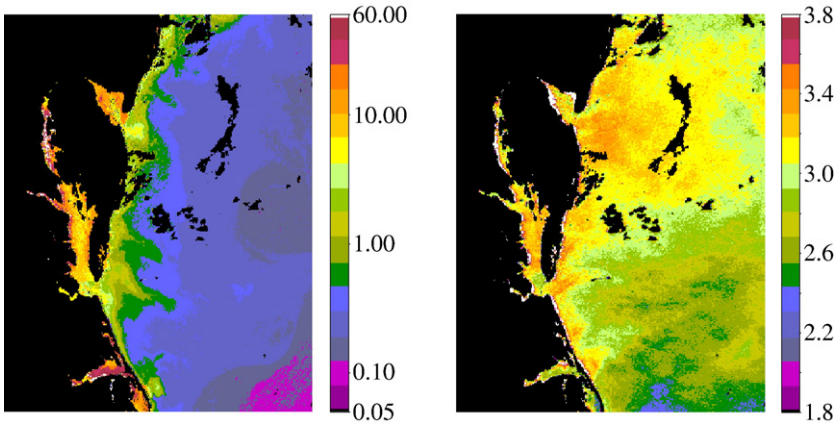

Fig. 7. Model SOA retrieved C (mg m^{-3}) and υ (dimensionless) for SeaWiFS, 22 Jul 1998.

5.4. SOA atmosphere and ocean decoupling

The SOA retrieves aerosol properties for optimal values of m_r and m_i in Eq. (8); namely the Junge size distribution parameter υ, optical depth $\tau(865)$ and single scattering albedo ω_0. i.e., a characterization of aerosol absorption is possible, distinguishing the SOA from StdGSM and Std. This study does not present a validation of the SOA in such atmospheres since none of the six scenes (see Table 2) appeared to contain areas of high aerosol absorption. The quantity ω_0 was usually between 0.98 and 1.0 in CB, with a maximum of 5% of pixels in the range 0.96 to 0.97.

To illustrate the decoupling of atmosphere and water parameters in this study, Fig. 7 displays SOA output for C and υ for 22 Jul 1998. A larger υ indicates smaller aerosol particles. The most striking feature of the aerosol image is the apparent plumes extending from the coast. Comparison of both images indicates successful decoupling for regions very near the coast and CB. For example, the structure of water features along the coast is not apparent in the aerosol plumes. The same is true for comparison of υ and the leftmost CDM image in Fig. 6. Both absorbers have successfully decoupled from the atmosphere in CB.

The scenes in Fig. 7 are expanded into the MAB to show a portion of the Gulf Stream in the lower right part of the chlorophyll *a* image. In this region lower υ suggests larger particles characteristic of maritime conditions. Decoupling here also appears complete. Other scenes not shown here do indicate small components of the Gulf Stream apparent in the aerosol structure.

The SOA aerosol retrieval pattern is also consistent with the wind speed and direction on the 22 July 1998, particularly at the mouth of CB. Wind data was obtained from the National Oceanic and Atmospheric Administration's National Data Buoy Center. Three stations were examined, CHLV2 (Chesapeake Light 36.91N 75.71W), 44009 (Delaware Bay 38.46N 74.7W) and 44014 (Virginia Beach 36.61N 74.84W). The first station is approximately 16 km ESE of the mouth of CB. The second two stations north and south of the mouth, some 41 and 104 km seaward from the coast respectively. The mean eight minute wind speed at each station for the same hour as the SeaWiFS overpass was 4.4, 4.8 and 4.6 m s^{-1}. The wind direction (clockwise from true north) is 216, 230 and 228° respectively. The direction of the aerosol plumes in rightmost Fig. 7 is well matched with the wind observations, particularly the two υ plumes at the mouth and to the north, both extending some distance from the coast.

6. Concluding remarks

In this case study we have applied both the spectral optimization algorithm and the standard atmospheric correction to the Chesapeake Bay using SeaWiFS imagery. The SOA contains a suite of aerosol models covering a wide range of aerosol absorption and a semi-analytic bio-optical model that encapsulates phytoplankton and CDM absorption. The standard atmospheric correction uses OC4v4 (which together are called the standard algorithm) and was also modified to replace OC4v4 with the same semi-analytic bio-optical model used in SOA. The semi-analytic model was parameterized to Chesapeake Bay using the most reliable sources of *in situ* information, and some of this *in situ* data set was compared with retrievals using the three models. The study produced several significant outcomes:

(1) The SOA and standard algorithm determine C to reasonable accuracy. In the *upper* bay the model comparisons are inconclusive with both Std and SOA suffering from some noise and inconsistently high values on 20 to 30% of occasions. The SOA does appear to be more accurate than Std in the *middle* and *lower* regions of CB for the *in situ* data used in this study. This is believed to result from the inclusion of CDM formulation and parameterization in SOA. For the *inshore* region, the *in situ* data bisects the lower SOA and higher Std values. If we replace band ratio algorithm OC4v4 by GSM-CB in the standard algorithm then results are poor for most of the data, particularly in the *upper* bay for 95% of pixels. However, histograms of C retrieval shown in the study indicate that if the failures are removed from StdGSM, then both SOA and StdGSM are similar in distribution shape.

(2) The SOA provides a robust CDM retrieval for the *upper*, *middle* and *lower* regions of the bay. This may not be surprising in the *upper* bay where 1) the dynamic range of a_{CDM} is possibly lower and more stable than a_{ph} and 2) a_{CDM} dominates over a_{ph}. The first phenomenon improves the aliasing of *in situ* data, while the second improves the optimization of a_{CDM} versus a_{ph} since the former is of higher magnitude. The performance of StdGSM is once again degraded, and of course, the Std does not retrieve a_{CDM}. Results for SOA retrieval of CDM in the *inshore* region appear degraded; however this is explained by the lack of *in situ* information and bio-optical model error.

(3) The decoupling of oceanic and atmospheric parameters was successful in CB for all six images used in this study. One of these scenes was illustrated. An important advantage of SOA is the inclusion of both visible and NIR bands in the atmospheric model, allowing for assessment of aerosol absorption for a particular scene. However, any benefit of the inclusion of absorbing aerosols in the SOA atmospheric correction was not divulged in this study due to insufficient availability of absorbing aerosol scenes. The extension of this work to more absorbing atmospheres is immediate, but remains untested.

The results imply that there can be no 'universal' Case 2 bio-optical set of coefficients in Chesapeake Bay. Robust retrieval of parameters required the regional variability in bio-optical properties. This has wider implications for other Case 2 regions: if investigators wish to use satellite imagery for a specific Case 2 area, it is likely they will have to develop their own customized set of bio-optical properties that apply specifically to that area.

Acknowledgements

Thanks to Mike Mallonee for assistance with *in situ* data collection. This work was prepared by University of Miami under contracts #NNG04HZ21C and NNX08AH93A from NASA and award #NA17RJ1226 from NOAA/NESDIS, U.S. Department of Commerce. The statements, findings, conclusions and recommendations are those of the authors and do not necessarily reflect the views of NASA, NOAA/NESDIS or the U.S. Department of Commerce.

References

Arnone, R. A., Martinolich, P., Gould, R. W., Jr., Stumpf, R., & Ladner, S. (1998). Coastal optical properties using SeaWiFS. In S. Ackleson & J. Campbell (Eds.), *SPIE proceedings, ocean optics XIV* Washington, DC: Office of Naval Research.

Carder, K. L., Chen, F. R., Lee, Z. P., Hags, S. K., & Kamykowski, D. (1999). Semi analytic Moderate Resolution Imaging Spectrometer algorithms for chlorophyll *a* and absorption with bio-optical domains based on nitrate-depletion temperatures. *Journal of Geophysical Research*, *104C*, 5403–5421.

Chomko, R. M., & Gordon, H. R. (1998). Atmospheric correction of ocean color imagery: Use of the Junge power-law aerosol size distribution with variable refractive index to handle aerosol absorption. *Applied Optics*, *37*, 5560–5572.

Chomko, R. M., & Gordon, H. R. (2001). Atmospheric correction of ocean color imagery: Test of the spectral optimization algorithm with the Sea-viewing Wide Field-of-View Sensor. *Applied Optics*, *40*, 2973–2984.

Chomko, R. M., Gordon, H. R., Maritorena, S., & Siegel, D. A. (2003). Simultaneous retrieval of oceanic and atmospheric parameters for ocean color imagery by spectral optimization: A validation. *Remote Sensing of Environment*, *84*, 208–220.

Ding, K., & Gordon, H. R. (1995). Analysis of the influence of O_2 A-band absorption on atmospheric correction of ocean-color imagery. *Applied Optics*, *34*, 2068–2080.

Gallegos, C.L., Smithsonian Environmental Research Center, Edge water, MD 20771, USA, personal communication (2006).

Gallegos, C. L., Jordan, T. E., Hines, A. H., & Weller, D. E. (2005). Temporal variability of optical properties in a shallow, eutrophic estuary: Seasonal and interannual variability. *Estuarine, Coastal and Shelf Science*, *64*, 156–170.

Garver, S. A., & Siegel, D. A. (1997). Inherent optical property inversion of ocean color spectra and its biogeochemical interpretation: 1 time series from the Sargasso Sea. *Journal of Geophysical Research*, *102C*, 18607–18625.

Gordon, H. R. (1997). Atmospheric correction of ocean color imagery in the Earth Observing System era. *Journal of Geophysical Research*, *102*(D14), 17081–17106.

Gordon, H. R., Brown, O. B., Evans, R. E., Brown, J. W., Smith, R. C., Baker, K. S., et al. (1988). A semi-analytic radiance model of ocean color. *Journal of Geophysical Research*, *93*(D9), 10909–10924.

Gordon, H. R., Du, T., & Zhang, T. (1997). Remote sensing ocean color and aerosol properties: Resolving the issue of aerosol absorption. *Applied Optics*, *36*, 8670–8684.

Gordon, H. R., & More, A. Y. (1983). *Remote assessment of ocean color for interpretation of satellite visible imagery: A review.* Springer-Verlag, New York.

Gordon, H. R., & Wang, M. (1994a). Retrieval of water-leaving radiance and aerosol optical thickness over the oceans with SeaWiFS: A preliminary algorithm. *Applied Optics*, *33*, 443–452.

Gordon, H. R., & Wang, M. (1994b). Influence of oceanic whitecaps on atmospheric correction of SeaWiFS. *Applied Optics*, *33*, 7754–7763.

Harding, L. W., Jr., Magnuson, A., & Mallonee, M. E. (2004). SeaWiFS retrievals of chlorophyll in Chesapeake Bay and the Mid-Atlantic Bight. *Estuarine, Coastal and Shelf Science*, *62*, 75–94.

Kuchinke, C. P., Gordon, H. R., & Franz, B. A. (2009). Spectral optimization for constituent retrieval in Case 2 waters I: Implementation and performance.*Remote Sensing of Environment*, *113*, 571–587 doi:10.1016/j.rse.2008.11.001.

Loisel, H., Nicolas, J. M., Sciandra, A., Stramski, D., & Poteau, A. (2006). Spectral dependency of optical backscattering by marine particles from remote sensing of the global ocean. *Journal of Geophysical Research*, *111*, C09024.

Magnuson, A., Harding, L. W., Jr., Mallonee, M. E., & Adolf, J. E. (2004). Bio-optical model for Chesapeake Bay and the Middle Atlantic Bight. *Estuarine, Coastal and Shelf Science*, *61*, 403–424.

Maritorena, S., Institute for Computational Earth System Science, 6841 Ellison Hall, UCSB, Santa Barbara, CA 93106, USA, personal communication (2005).

Maritorena, S., Siegel, D. A., & Peterson, A. R. (2002). Optimization of semi-analytical ocean color model for global scale applications. *Applied Optics*, *41*, 2705–2714.

Morel, A. (1974). Optical properties of pure water and pure sea water. In N. G. Jerlov & E. S. Nielson (Eds.), *Optical aspects of oceanography* (pp. 1–24). San Diego, Calif: Academic.

Moulin, C., Gordon, H. R., Chomko, R. M., Banzon, V. F., & Evans, R. H. (2001). Atmospheric correction of ocean color imagery through thick layers of Saharan dust. *Geophysical Research Letters*, *28*, 5–8.

O'Reilly, J. E., Maritorena, S., Mitchell, B. G., Siegel, D. A., Carder, K. L., Garver, S. A., et al. (1998). Ocean color chlorophyll algorithms for SeaWiFS. *Journal of Geophysical Research*, *103*, 24,937–24,953.

Pope, R. M., & Fry, E. S. (1997). Absorption spectrum (380–700 nm) of pure water. 2. Integrating cavity measurements. *Applied Optics*, *36*, 8710–8723.

Ruddick, K. G., Ovidio, F., & Rijkeboer, M. (2000). Atmospheric correction of SeaWiFS imagery for turbid coastal and inland waters. *Applied Optics*, *39*, 897–912.

Siegel, D. A., Wang, M., Maritorena, S., & Robinson, W. (2000). Atmospheric correction of satellite ocean color imagery: The black pixel assumption. *Applied Optics*, *39*(21), 3582–3591.

Tzortziou, M., Herman, J. R., Gallegos, C. L., Neale, P. J., Subramaniam, A., Harding, L. W., Jr., et al. (2006). Bio-optics of the Chesapeake Bay from measurements and radiative transfer closure. *Estuarine, Coastal and Shelf Science*, *68*, 348–362.

Yang, H., & Gordon, H. R. (1997). Remote sensing of ocean color: Assessment of the water-leaving radiance bidirectional effects on the atmospheric diffuse transmittance. *Applied Optics*, *36*, 7887–7897.